Journal of Food Engineering 117 (2013) 59–66

Contents lists available at SciVerse ScienceDirect

Journal of Food Engineering

journal homepage: www.elsevier.com/locate/jfoodeng

Development of a portable hyperspectral imaging system for monitoring the efficacy of sanitation procedures in food processing facilities

Alan M. Lefcourt [a,*], Michael S. Wiederoder [a,b], Nancy (Tong) Liu [a,b], Moon S. Kim [a], Y. Martin Lo [b]

[a] USDA, Agricultural Research Service, Environmental Microbial and Food Safety Laboratory, Bldg. 303, Beltsville, MD 20705, USA
[b] Department of Nutrition and Food Science, University of Maryland, College Park, MD 20740, USA

a r t i c l e i n f o

Article history:
Received 3 October 2012
Received in revised form 30 January 2013
Accepted 31 January 2013
Available online 8 February 2013

Keywords:
Hyperspectral imaging
Fluorescence imaging
Food safety
Sanitation inspection
Portable

a b s t r a c t

Cleaning and sanitation in food processing facilities is a critical step in reducing the risk of transfer of pathogenic organisms to food consumed by the public. Current methods to check the effectiveness of sanitation procedures rely on visual observation and sub-sampling tests such as ATP bioluminescence assays and culturing methods. To augment existing verification methods, a hand-held visible hyperspectral imaging device was developed. The device is capable of acquiring reflectance images using ambient lighting, and fluorescence responses to supplemental violet (405 nm) excitation. To enhance the ability of detecting relatively low intensity fluorescence responses in the presence of ambient lighting, the device includes the ability to identify wavebands where the intensity of ambient lighting is relatively low. Valleys in ambient illumination intensity when using fluorescent lighting were found at around 475, 520, 570, and 675 nm. A principal goal is to acquire data to support development of a commercially-viable, hand-held, imaging system.

1. Introduction

The recognized risks and increased public awareness concerning food safety led to the Food Safety Modernization Act of 2011 (FDA, 2012; Taylor, 2011). Two important consequences of this act are an increase in the authority of the FDA to suspend the licensing of problematic facilities as opposed to simply recalling tainted products, and an increased emphasis on process control as opposed to commodity inspection. Process control generally involves development and use of HACCP (Hazard Analysis and Critical Control Points) protocols designed to reduce the incidence of foodborne illness by identifying and mitigating risk factors (Hulebak and Schlosser, 2002; FDA, 2011). Compliance measures normally include some aspect of visual observation. Consider cleaning and sanitation, ATP bioluminescence assays and microbiological sampling are used as spot checking techniques, but the primary method for checking the efficacy of cleaning efforts is visual observation (Cunningham et al., 2011; Leon and Albrecht, 2007; Poulis et al., 1993; Pérez-Rodríguez et al., 2008).

The potential always exists to improve on human vision using imaging technologies. The interest and use of hyperspectral imaging in agricultural has accelerated in recent years and has demonstrated that imaging in the visible (VIS) spectrum can be the basis for sensitive methods for addressing agricultural problems (Kim et al., 2011; Zhang et al., 2012). The goal of this project is to develop a hand-held imaging system that incorporates both reflectance and fluorescence capabilities, can be used to acquire hyperspectral VIS data, and is sufficiently robust for use in commercial food processing facilities. The ultimate goal is to garner data that allows development of a cost-effective, hand-held, imaging system with commercial viability.

A major concern with imaging systems is potential false positives, particularly if the imaging device is designed for use by non-technical personnel. For this reason, research efforts are directed towards developing an imaging device that can be used to investigate the efficacy of cleaning and sanitation protocols. The advantage is that it can be assumed that any anomaly detected following cleaning and sanitation, including residuals from normal product, represents a potential problem.

Trial-and-error played a major role in the development of the imaging system. The description of the system emphasizes operating characteristics that proved to be effective. Discussion emphasizes factors that played a role in the development of the system.

2. Materials and methods

2.1. Portable hyperspectral system

The portable hyperspectral imaging system (Figs. 1–4) consists of a C-mount lens (Rainbow S16mm, 2/3″, Sensei Shoj Co., Japan), a liquid–crystal tunable filter (400–720 nm, 20 nm FWHM (Full

* Corresponding author. Tel.: +1 301 504 8450x258; fax: +1 301 504 9466.
E-mail address: alan.lefcourt@ars.usda.gov (A.M. Lefcourt).

0260-8774/$ - see front matter © 2013 Elsevier Ltd. All rights reserved.
http://dx.doi.org/10.1016/j.jfoodeng.2013.01.043

Fig. 1. Imaging system in use, showing camera system head mounted on a tripod and backpack containing batteries, laptop, and filter controller.

Width at Half Maximum); VariSpec VIS, Caliper Life Sciences, USA), back-correction optics (Channel Systems Inc., Canada), and a monochrome CCD camera (Prosilica GC1380, Allied Vision Technologies, Germany). To better accommodate the narrow view angle of the tunable filter, the filter is placed between the lens and the camera. The back correction optics provide the necessary adjustment for focal distance accordingly. Static or video images are displayed using a small touch-screen monitor (7″; 705TSV, Xenarc Technologies Corp., USA) attached to the device. Rechargeable lithium-ion battery packs (6 V, 10 A h {Ampere–hour}; ONLYBATTERYPACKS, USA), a laptop computer (D430, Dell, USA), and tunable filter controller are housed in a backpack, which is tethered to the camera system head. Three battery packs are wired in series to provide 18 V for illumination, and tapped to provide 12 V for the camera and monitor. Software[1] written in Visual Basic Version 6 (Microsoft, USA) is used to control the tunable filter, to capture images, and for on-site analyses. A commercial SDK (Software Development Kit) is used for image acquisition (ActiveGigE, A&B Software, USA).

To provide some protection from the environment, components in the camera head that do not need to be exposed are enclosed in a metal box and box junctions are sealed using vinyl electrical tape. When used in cold environments, a desiccant canister (45 gm Reusable Desiccant Canister, DesiccantsOnline, USA) is attached inside the box using Velcro. To allow acquisition of hyperspectral data, which requires that the camera remain in the same position for a short period of time, the camera head includes a tripod mounting bracket. The bracket is connected to a pistol grip (AF2100, Silk, Japan), which in turn is connected to a tripod (3021BPro, Manfrotto Distribution Inc., USA). In use, the pistol grip always remains attached to the camera head. A quick-connect coupling allows the grip to be attached and detached from the tripod. When attached, the grip trigger allows the camera head to be positioned using the grip's ball-mount.

For fluorescence-based detection, a switch is used to activate four 10-watt, 405 nm, LEDs (LED Engin, USA). Power for the LEDs is from four constant current sources, which are wired in series (BuckPuck 700 ma, LuxDrive, USA). To help dissipate heat, each LED is mounted in an aluminum finned casing (E27 LED Casing, DealExtreme, Hong Kong); to better homogenize and direct the illumination, diffuser lenses are incorporated in casings (35 mm Optical Diffuser, DealExtreme). To further dissipate heat, the casings are mounted on a thin aluminum sheet that is offset 10 mm from the main camera head (Fig. 4). Images can be acquired with and without the supplemental violet illumination, and difference images displayed.

2.1.1. Image characteristics

The native resolution of the camera is 1360 (H) × 1024 (V) pixels. Acquired images are binned in both dimensions by three to yield an effective resolution of 453 × 341 pixels. This resolution allows images to be displayed in their entirety on the touchscreen monitor, which has a resolution of 800 × 480 pixels. Binned images are saved in TIF 16-bit grayscale format to preserve the full 12-bit resolution of the camera CCD. During image acquisitions, only the most significant 8-bits are displayed. For off-line analyses, the full 12-bit images are used and resultant images are scaled to 8-bits for display.

2.2. Operation

Operational functions are selected by pressing the appropriate icon on the touchscreen (Fig. 4). Most actions are direct; however, some icons bring up additional screen forms. Only the more critical functions are outlined below.

2.2.1. Gain

Autogain is disabled in the camera to ease comparison of results across locations and time. To maximize dynamic range in images, the exposure time is normally the inverse of the frame rate (default: 15 frames per s) with a small adjustment made for data transfer timing. An automated routine allows an array of gains to be calculated and stored at 5 nm intervals from 400 to 720 nm, inclusive. The routine adjusts the gain at a particular wavelength until the average pixel intensity of the center region of the image is just less than a selected threshold, normally 1024. The points used to define the coordinates of the center region are the points one-third and two-thirds the distance along the horizontal and vertical image dimensions. The camera directly supports integer gains of 0–32. Negative gains are implemented in software by using a hardware gain of zero and reducing exposure time using the empirically-derived formula:

$$\text{ExposureTime} = \text{MaximumExposureTime}/(2\hat{}(7 * |\text{Gain}|/12))$$

where MaximumExposureTime is the maximum exposure time that can be implemented for the current frame acquisition rate. The formula is an exponential function modified to mimic the extension of the hardware gain in terms of changes in the average measured intensity of a white HDPE cutting board under ambient fluorescent lighting. Pressing the "Gain" icon (Fig. 4) brings up a form that graphically displays gains by wavelengths for five named gain profiles: "HDPE Fixed", "SS Fixed" (Stainless Steel), "General", "HDPE", and "SS" along with the name of the profile currently in use. Profile names are arbitrary, and are meant only to ease identification of displayed profiles. The user is asked to select the gain profile to be used and, for the last three profiles, whether the gain array for the selected profile should be recalculated. Each time a gain array for a profile is recalculated, a corresponding text file is written to disk. The most recent file for each profile is read when the system is turned on. For this study, the "HDPE Fixed" and the "SS Fixed" profiles were renamed "Gain 0" and "Gain −4", and the associated gain arrays were assigned uniform values of 0 or −4, respectively.

2.2.2. Scanning image acquisition

For single wavelength acquisitions, there are a number of methods that can be used to select the acquisition wavelength,

[1] Copies of the Visual Basic software, without warranty, are available from the authors upon request.

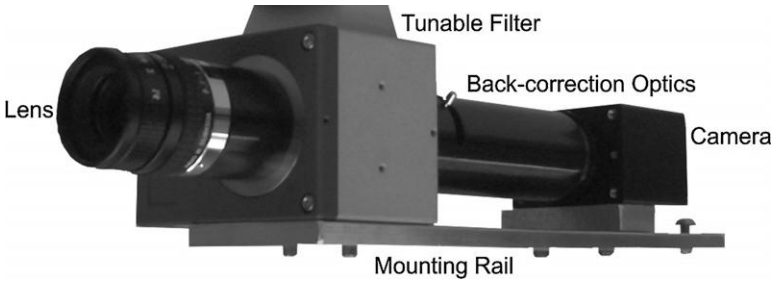

Fig. 2. Core camera system components, including lens, tunable filter, back-correction optics, camera, and aluminum mounting rail.

Fig. 3. Switch controlled illumination components, including 405 nm LEDs, heat dissipating casings, and glass diffusion lenses.

including pressing the "〈" or "〉" icon (Fig. 4). In addition, there are four icons that control flags important for scanning image acquisition. The "Cycle 3" icon allows image acquisition to be cycled through three selected wavelengths; the "Cycle All" cycles through all wavelengths within a selected range. The defaults are 475, 520, and 675 nm, and 465–695 nm at 10 nm intervals, respectively. All cycling parameters, including display dwell time (default: one sec), are user selectable. The "Save Movie" icon allows acquired images to be stored to disk. For single wavelength acquisitions, the storage rate is selectable with a default rate of one frame per sec. If a "Cycle" icon is selected, one frame per wavelength per cycle is stored. The "Save Image" icon allows a single image to be saved.

2.2.3. Hyperspectral image acquisition

The "Hyper Differ." icon (Fig. 4) allows selection of hyperspectral imaging. For this case, the camera head has to remain in a set position while a series of images at five nm intervals from 460 to 720 nm are acquired first with and then without LED illumination. The manual switching of the LEDs on and then off is confirmed by selecting the appropriate icon. A small time delay is added to address camera jitter when icons are pressed. After all images are acquired, the images are read from disk, and then difference images by wavelength are calculated, scaled, and cycled.

2.2.4. Ancillary display information

The primary screen display includes the current time, the calculated frame rate, and the temperature of the tunable filter (Fig. 4). Information about the current image being displayed also includes whether the illumination is on, the wavelength, the gain, and the intensity at a selected pixel location. The pixel location can be selected when the image is not cycling by tapping the image at the desired location. For fine location control, a pointer housed in the back of the monitor can be used. When cycling, tapping the image stops and restarts the cycling process.

Fig. 4. Picture of the touch screen monitor showing control icons and an image acquired at 470 nm with violet LED illumination. The faint white lines are knife slices on the HDPE (High-density Polyethylene) cutting board, the darker corners reflect the limitations of the tuning filter, and the text indicating intensity sampling location (x,y), sampled intensity (inten.), system temperature (tempt.), and frames per s (fps) were added for clarification.

2.2.5. Setup and analyses

Pressing the "Setup" icon (Fig. 4) suspends the image acquisition process and brings up a screen where operating parameters can be changed. This screen includes the "Analysis" icon that can be used to bring up the analysis screen where acquired images can be transformed and reviewed. Transforms include scaling, image ratios, and image differences. It is possible to automatically cycle through various transforms. More detailed information regarding these screens is not provided as the screens were seldom used during actual visits to processing plants (Wiederoder et al., accepted for publication).

2.3. Testing

To test the effectiveness of heat dissipation mechanisms for LED illumination, the temperature was measured at 1 min intervals and the intensity of illumination at 5 s interval after turning on the LEDs. LED temperature was estimated using an electronic thermometer (Model HH502; Omega Engineering, USA) and a K-type thermocouple attached to the aluminum plate directly behind the center location of one of the four LEDs using heat sink compound. The illumination intensity was measured at 415 nm using a white HDPE cutting board as the target and the intensity measurement procedure developed for setting camera gain.

To test the wavelength accuracy of the tunable filter, hyperspectral images of five fluorescence standards were acquired. Standards with peaks at 460 nm (USFS-200-020), 540 nm (USFS-210-020), and 590 nm (USFS-336-020); and at 515 nm (FCC-02GPU) and 660 nm (FFC-02HRU) were obtained from Labsphere (USA) and Avian Technologies (USA), respectively. The 540 and 660 nm standards have secondary peaks at 560 and 625 nm, respectively. Spectra were calculated by averaging the intensity of each standard at each measured wavelength using a circle mask that represented about 90% of the surface area and was centered on the standard.

3. Results and discussion

3.1. State of the art

Over the last 10 years, interest has grown in the use of hyperspectral fluorescence imaging to address agricultural problems (Kim et al., 2011; Zhang et al., 2012). However, literature concerning handheld hyperspectral imaging systems in agriculture is non-existent. A commercial handheld, single wavelength, fluorescence-based imaging system was used to examine the existence and origination of fecal contamination on carcasses during slaughter (Burfoot et al., 2011). Kim et al. (2012) was awarded a patent for a hand-held inspection tool.

The potential application that was used to frame design considerations for the imaging system was inspection following routine cleaning and sanitation procedures in fresh-cut processing plants. Surface contamination, and determining the efficacy of cleaning efforts, is an identified problem in produce processing facilities (Lehto et al., 2011). Focusing on the problem of inspection following cleaning reduces concerns regarding false positives; residues from production can be considered to be an indication of incomplete cleaning and the immediacy of imaging results allows workers to examine the realness of a suspect site by re-cleaning and reexamination. In addition, imaging should increase the efficacy of sub-sampling tests by identifying questionable locations for testing. A laboratory study of produce residues demonstrated that the residues could be detected at multiple wavelengths against a background of HDPE or SS, and that cleaning and sanitizing agents would not lead to false positives (Wiederoder et al., 2012). A study using the device described herein for sanitation inspection in produce processing plants has been published (Wiederoder et al., accepted for publication).

3.2. System design considerations

3.2.1. Selection of camera and filter

The camera was selected for sensitivity, low noise level, 12-bit minimum resolution, Gigabit Ethernet interface, size, and cost. The filter was selected to allow full frame images to be acquired at any selected visible wavelength in real time. The tunable filter selected has some potential disadvantages. First, the technology includes a polarization step, which reduces light throughput. Second, the inherent view angle is narrow. The narrow view angle was addressed by placing the filter between the lens and the camera. Even so, the effective light throughput was greater at the center of images compared to edges. In practice, the affect of the throughput gradient was minimal as the natural tendency of users is to center the image on the area of interest.

3.2.2. Selection of fluorescence excitation source

The original intent was to use a halogen UV source. However, there are safety considerations for using intense UV illumination, particularly in relation to eye safety. Furthermore, the optimal excitation wavelength for inducing a fluorescence response from chlorophyll-a related substances is about 420 nm (Kim et al., 2003); thus, a decision was made to use violet LEDs for illumination. Safety considerations are reduced due to a direct reduction in potential harm from violet compared to UV radiation. Risk is further reduced because violet illumination is visible to the naked eye and there is a natural tendency to look away from a bright light source.

The LEDs selected for use have a wide dispersion angle (120°) necessitating the use of a mechanism such as a lens or a reflector to reduce the dispersion. The LEDs are also a significant heat source. The external, finned, heat sink casings were used to improve heat transfer from the hot LEDs. An external heat sink allows for both radiant heat transfer to the ambient atmosphere and convective heat transfer. Convective heat transfer is facilitated by air flow resulting from thermal-gradients along the heat sink and convective efficiency is increased by even very low velocity air movement such as occurs when the camera head is moved during surface scans. An alternative could be to use internal heat sinks. An internal heat sink generally requires use of an opening in the device to facilitate air flow across the heat sink and often requires use of a fan to guarantee adequate air flow; thus, complicating the cleaning of the device. The casing used for the imaging device is designed to incorporate standard lenses of various types. The lens selected for use provides a good tradeoff between uniformity and efficiency for illuminating the area of interest.

The illumination intensity of LEDs naturally decrease as a function of operating temperature. To test the efficiency of the heat dissipation mechanisms, the temperature above one LED casing and illumination intensity were measured over time (Fig. 5). To mimic movement of the camera head, the test was conducted in a room where the air conditioner fan was constantly on and the camera head was subject to light air flow, i.e., air flow was just detectable using an exposed forearm. The temperature stabilized at about 54 °C after about 15 min with the illumination at 83% of the initial intensity. For comparison, values interpolated from the radiant flux graph provided by the LED manufacturer are 72% and 35% at 54 °C and 100 °C, respectively.

3.2.3. Backpack configuration

The primary factor in the decision to use a backpack was the weight of the camera head. A number of backpacks and hip packs were evaluated. The selected backpack interfered less with normal

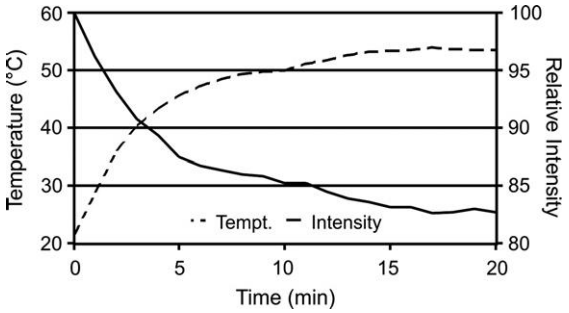

Fig. 5. Rise in LED temperature and fall in relative excitation intensity versus on-time. Note that the system reached steady-state in about 15 min with a 17% loss in illumination intensity.

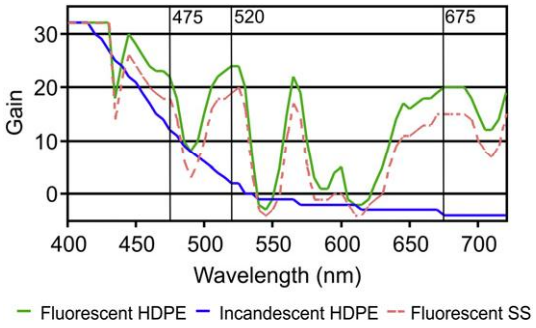

Fig. 6. Gain profiles by wavelength acquired using either fluorescent or incandescent ambient lighting with white HDPE or stainless steel as the target. The 475, 520, and 675 nm wavelengths are the default wavelengths used for auto cycling.

movements and included two compartments, one used for the battery packs and the other for the computer and filter controller. The original design criteria stipulated that the batteries had to support 2 hours of continuous use. This criterion can be met using 3–5 A h battery packs. With battery weight no longer a limiting factor, 10 A h battery packs were used instead.

The choice to use a backpack also influenced the selection of the laptop. The original laptop was replaced with the Dell laptop because the Dell laptop has an external power button and all connections are across the spine of the computer. The original laptop had connections along both sides of the computer and accessing the power switch required removing the laptop from the holder in the backpack and then opening the laptop.

3.2.4. Selection of monitor

The decision to use a backpack eliminated the requirement that computational abilities be included within the camera head and allowed the use of a simple touch screen monitor; alternatively, if a backpack was not used, a tablet PC could be used as the monitor. The criteria used to select the monitor were that it could be physically attached to the camera head, that it incorporated a touch screen, and that it was inexpensive. Thus, the camera head could be held in one hand and operation parameters set using the other hand and the monitor.

3.2.5. Operational considerations

A major consideration in the development of the portable hyperspectral imaging system was the expected low intensity of fluorescence responses and the consequential difficulty of detecting the responses against a background subject to ambient illumination. The default frame rate of 15 frames per s was selected as the best compromise between maximizing exposure time and reducing motion artifacts.

The decision to use a fixed camera gain as opposed to using either the camera hardware auto gain function or software to provide an automated gain function was based on a number of factors. First, it proved difficult to consistently identify the putative origin of a detected anomaly in an image when the brightness of that type of anomaly varied in images due to automated changes in camera gain. Second, automated gain adjustments frequently hindered visual detection of anomalies, particularly when the scene being imaged was dark or contained a very bright area. Third, the finite time delay in adjusting gains sometimes resulted in a positive feedback loop where the user would move the camera head in responses to the effects of the changing gain, which would then initiate a new round of gain change. Fourth, the time delay associated with waiting for automated gains to stabilize increased effective scanning times and times for acquiring hyperspectral data cubes. A single, selectable, gain setting proved to be impractical because of variations in ambient lighting intensity due to location within a facility and wavelength dependent differences associated with the type of ambient lighting used in the facility. The next software iteration used a single gain array where gains could be calculated and stored at 5 nm intervals. The use of a single gain profile proved impractical as gain profiles had to be recalculated frequently primarily due to changes in the composition of target backgrounds, e.g., HDPE exhibits an auto fluorescence response to supplemental LED illumination while SS does not. In the current software, users can select among five named gain profiles and, if desired, recalculate one of the three variable profiles by pressing the appropriate icon. The gain profiles are graphed to allow users to better select the appropriate gain array for use.

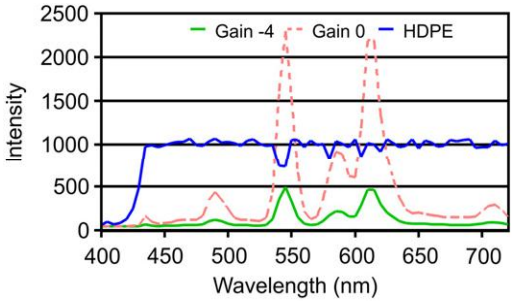

Fig. 7. Measured intensity as a function of wavelength using ambient fluorescent lighting and a white HDPE target by camera gain profile. Note that use of the Fluorescent HDPE (HDPE) gain profile shown in Fig. 6 results in a near uniform measured intensity of 1000.

The finding that all types of anomalies of interest could not be detected using a single wavelength resulted in the addition of the ability to automatically cycle among a set of preselected wavelengths. The addition of the ability to cycle was dependent on the development of automated gain profiles. The number of wavelengths used for cycling was eventually restricted to three as users had difficulty following more than three wavelengths. The ability to tap on the display to start and stop cycling facilitated the acceptance of the cycling option.

The three wavelengths used for cycling were selected by examining the wavelengths where ambient illumination was relatively low to see if a subset of these wavelengths could be used to detect all anomalies of interest. The 475, 520, and 675 nm wavelengths were selected based on an understanding of wavelengths appropriate for detecting organic residues (Wiederoder et al., 2012). When the device was tested in produce plants, the wavelengths were found both to be necessary and adequate for detecting all anomalies of interest, including defects in HDPE and SS surfaces (Wiederoder et al., accepted for publication). It should be noted

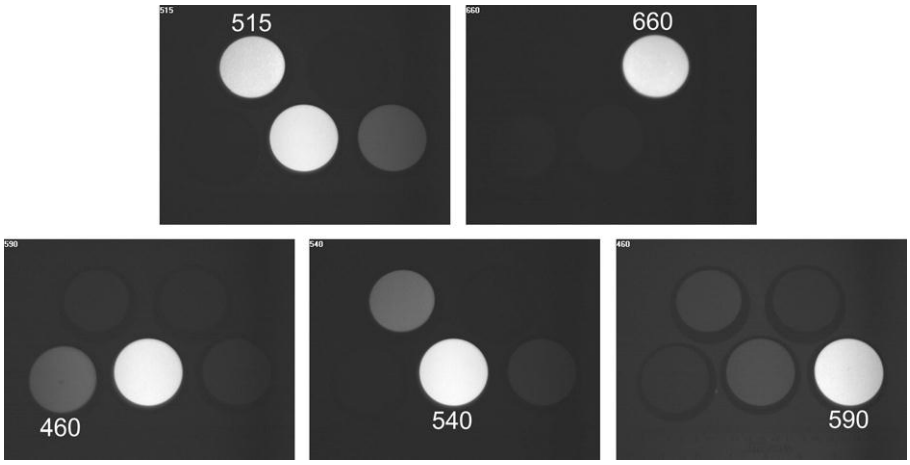

Fig. 8. Images of 460, 515, 540, 590, and 660 nm fluorescent standards acquired with LEDs on, gain set to −4, and ambient illumination off. A single standard is labeled in each of the five frames to allow identification of the locations of the standards and to indicate the waveband used to acquire that frame.

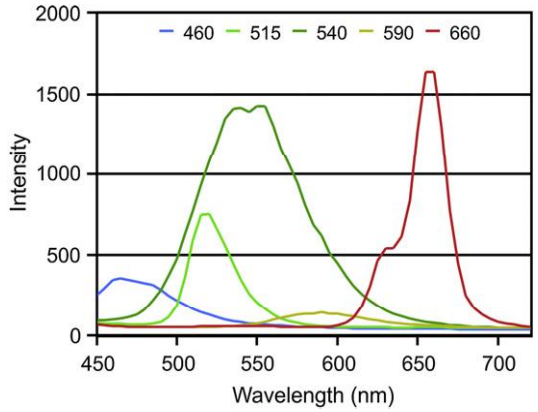

Fig. 9. The measured peaks of spectral responses to LED illumination of fluorescence standards (460 nm, 515 nm, 540 nm, 590 nm, and 660 nm; Fig. 8) correspond to the theoretical peaks. Note that ambient fluorescent lights were off and that the measured secondary peaks at 560 nm (540 nm standard) and 625 nm (660 nm standard) also correspond to theoretical secondary peaks.

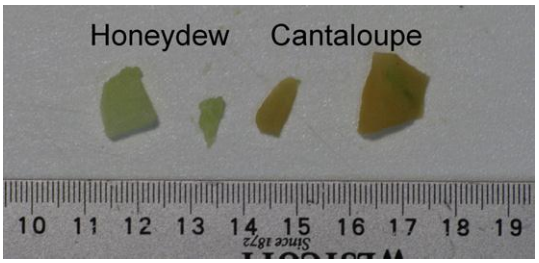

Fig. 10. Picture of melon pieces on HDPE used for hyperspectral imaging in Fig. 11.

that informal test results suggest that there is some leeway in the selection of wavelengths used for detection.

The original software included an icon on the main screen that allowed users to display images in real time that were created as a function of registered images acquired at two different wavelengths. It soon became evident that the major time cost for these operations was setting up the tripod and camera head. As the incremental time for acquiring a complete hyperspectral data cube was minimal, the two wavelength acquisition option was abandoned and the analyses routines were moved to a separate form where acquired hyperspectral data could be accessed. When the system was used in actual processing plants (Wiederoder et al., accepted for publication), onsite analyses were generally restricted to simple review of acquired images. In processing plants, the time window between cleanup and the start of the next production cycle is often less than 1 hour, and it was deemed more appropriate to concentrate on image acquisition.

3.3. System validation

3.3.1. Gain control

Gain profiles shown in Fig. 6 demonstrate effects of ambient lighting. A high gain corresponds to low ambient light intensity. The intensity for incandescent lighting shows a constant rate of rise from 400 to about 520 nm and then plateaus. For fluorescent lighting, there are peaks in gain that correspond to wavelengths where relative intensity of ambient lighting is low. The peaks at 475, 520, and 675 nm correspond to the default wavelengths for auto cycling. Gains rise again for wavelengths below 475 nm; however, there is spillover of reflected energy from the LEDs up to around 465 nm that precludes using these lower wavelengths for fluorescence imaging. The peak at around 570 nm suggests that 570 nm could also be a candidate wavelength for fluorescence imaging depending on target response characteristics. The time needed to acquire the necessary images and to calculate a new gain profile is approximately 40 s.

Fig. 7 demonstrates the ability of a gain profile to normalize measured intensity across wavelengths. Spectral responses using a white HDPE cutting board as the target were acquired using fixed camera gains of 0 and −4, and the HDPE Fluorescent gain array in Fig. 6.

3.3.2. Spectral response

Five fluorescent standards were used to examine the accuracy of the tunable filter (Fig. 8). Spectral responses of the standards are shown in Fig. 9. These results indicate that there is essentially no error in the ability to select wavelengths for imaging.

3.3.3. Performance characteristics

Fig. 10 is a color picture of pieces of honeydew and cantaloupe melon flesh on an HDPE cutting board. Fig. 11 shows images of the melon pieces at 475, 520, and 675 nm with the ambient fluorescent lights either on or off. Fig. 12 shows the melon spectra. The imaging data were acquired using the "Hyper Differ." icon (Fig. 4) with the hardware gain set to zero across wavelengths. The time to acquire a single hyperspectral data cube is about 11 s. The time to

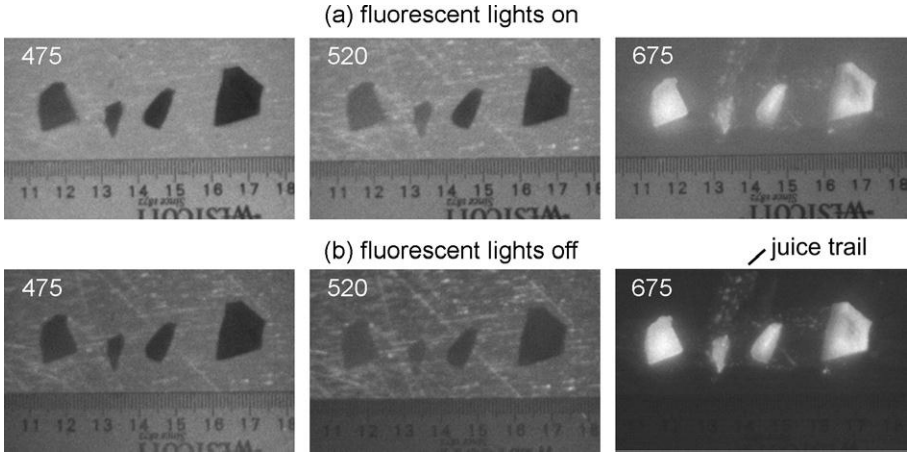

Fig. 11. Selected region of images of melon pieces at the three wavelengths commonly used for cycling. Images were acquired with LEDs on and room fluorescent lights either on (a) or off (b).

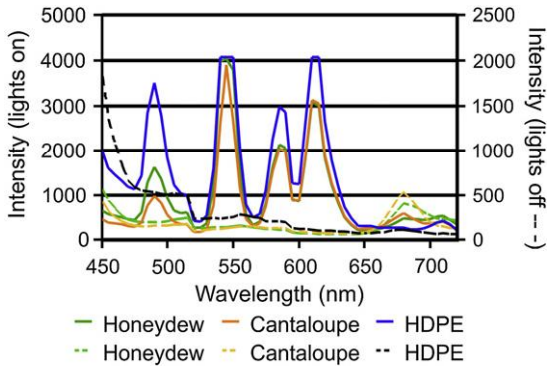

Fig. 12. Spectra of the two center melon pieces and a section of the HDPE surface with the fluorescent lights either on (solid lines) or off (dashed lines) with the gain set to zero.

acquire two data cubes, with and without LED illumination, and to calculate and display difference images is about 24 s plus any added display time for difference images.

The autofluorescence of HDPE from 450 to about 525 nm seen in Fig. 12 was noted in a prior laboratory study of produce residues (Wiederoder et al., 2012). As was discussed in this earlier study, this autofluorescence-based results in the melon pieces appearing black at 475 and 520 nm (Fig. 11). Under ambient fluorescent lighting, the contrast at 475 nm was greater than the contrast at 675 nm. This difference in contrast suggests that scanning could be done at a greater distance while using imaging at 475 nm to bringing attention to possible small pieces of produce residue. The camera head could then be brought closer to the suspected anomaly to allow examination at 675 nm.

The relatively brighter lines in images at 475 and 520 nm reflect cutting board use and are most likely knife cuts (Fig. 11). The contrast of these lines is greater in images at 520 nm. Although these lines do not necessarily represent a direct food safety concern, areas of concentrated use might be good sites for ATP testing.

The melon pieces were easily identifiable at 675 nm, even when ambient fluorescent lights were on (Fig. 11). The juice trails evident in the 675 mm images were created when melon pieces were positioned in a row using a knife tip. The trails were not visible to the naked eye in the absence of violet excitation, and were only faintly visible with violet excitation when the ambient lights were turned off. The pieces were cut on a different cutting board, transferred to a paper cup, and then placed on the imaging cutting board by lifting them out of the cup. Thus, the juices shown in images are primarily the result of "damage" resulting from dragging the pieces across the cutting board surface. The ability to see the trails in the 675 nm images is indicative of the sensitivity of the imaging device.

4. Conclusions

Tests of the handheld hyperspectral imaging system demonstrate that the system can acquire spectra at 5 nm intervals from 460 to 720 nm in about 11 s, and that fluorescence-based responses to violet LED excitation can be detected under ambient fluorescent lighting by utilizing wavelengths, such as 475, 520, and 675 nm, where the intensity of ambient lighting is relatively low. By automatically cycling through these three wavelengths, the system can be used to detect wear on HDPE surfaces as well as the presence of produce residues. These characteristics along with sensitivity of the system, demonstrated by the ability to easily detect small quantities of juice released when pieces of honeydew or cantaloupe melon were repositioned on a HDPE cutting board, suggest that the instrument will be a valuable tool for assessing the efficacy of cleaning and sanitation procedures.

Acknowledgments

This work was funded by the USDA. Partial support for Michael S. Wiederodear and Nancy Liu was provided by the Department of Nutrition and Food Science, University of Maryland, College Park. The USDA is an equal opportunity employer.

References

Burfoot, D., Tinker, D., Thorn, R., Howell, M., 2011. Use of fluorescence imaging as a hygiene indicator for beef and lamb carcasses in UK slaughterhouses. Biosystems Engineering 109 (3), 175–185.

Cunningham, A.E., Rajagopal, R., Lauer, J., Allwood, P., 2011. Assessment of hygienic quality of surfaces in retail food service establishments based on microbial counts and real-time detection of ATP. Journal of Food Protection 74 (4), 686–690.

FDA., 2011. Food safety: Hazard Analysis & Critical Control Points (HACCP). <http://www.fda.gov/Food/FoodSafety/HazardAnalysisCriticalControlPointsHACCP/default.htm> (accessed 20.07.2012).

FDA., 2012. Food Safety Modernization Act (2011). <http://www.fda.gov/Food/FoodSafety/FSMA/default.htm> (accessed 20.07.2012).

Hulebak, K.L., Schlosser, W., 2002. Hazard analysis and critical control point (HACCP) history and conceptual overview. Risk Analysis 22 (3), 547–552. http://dx.doi.org/10.1111/0272-4332.00038.

Kim, M.S., Lefcourt, A.M., Chen, Y.R., 2003. Optimal fluorescence excitation and emission bands for detection of fecal contamination. Journal of Food Protection 66 (7), 1198–1207.

Kim, M.S., Chao, K., Chan, D.E., Yang, C., Lefcourt, A.M., Delwiche, S.R., 2011. Hyperspectral and multispectral imaging technique for food quality and safety inspection. In: Cho, Y., Kang, S. (Eds.), Emerging Technologies for Food Quality and Food Safety Inspection. CRC Press, New York, NY, pp. 207–234.

Kim, M.S., Lefcourt, A.M., Chao, K., Chen, Y.R., Senecal, A.G., Marek, P., 2012. Hand-held inspection tool and method. US patent number 8,310,544 B2.

Lehto, M., Kuisma, R., Määttä, J., Kymäläinen, H.R., Mäki, M., 2011. Hygienic level and surface contamination in fresh-cut vegetable production plants. Food Control 22 (3), 469–475.

Leon, M.B., Albrecht, J.A., 2007. Comparison of adenosine triphosphate (ATP) bioluminescence and aerobic plate counts (APC) on plastic cutting boards. Journal of Food Service 18 (4), 145–152. http://dx.doi.org/10.1111/j.1745-4506.2007.00060.x.

Pérez-Rodríguez, F., Valero, A., Carrasco, E., García, R.M., Zurera, G., 2008. Understanding and modelling bacterial transfer to foods: a review. Trends in Food Science and Technology 19 (3), 131–144.

Poulis, J.A., de Pijper, M., Mossel, D.A.A., Dekkers, P.Ph.A., 1993. Assessment of cleaning and disinfection in the food industry with the rapid ATP-bioluminescence technique combined with the tissue fluid contamination test and a conventional microbiological method. International Journal of Food Microbiology 20 (2), 109–116. http://dx.doi.org/10.1016/0168-1605(93)90098-2.

Taylor, M.R., 2011. Will the Food Safety Modernization Act help prevent outbreaks of foodborne illness? New England Journal of Medicine 365. http://dx.doi.org/10.1056/nejmp1109388 (e18(1)–e18(3)).

Wiederoder, M.S., Lefcourt, A.M., Kim, M.S., Lo, Y.M., 2012. Detection of fresh-cut produce processing residues on food contact surface materials using hyperspectral imaging. Journal of Food Measurement and Characterization 6 (1–4), 48–55. http://dx.doi.org/10.1007/s11694-012-9132-1.

Wiederoder, M.S., Liu, N., Lefcourt, A.M., Kim, M.S., Lo, Y.M., accepted for publication. Use of a portable hyperspectral imaging system for monitoring the efficacy of sanitation procedures in produce processing plants. Journal of Food Engineering.

Zhang, R., Ying, Y., Raoa, X., Li, J., 2012. Quality and safety assessment of food and agricultural products by hyperspectral fluorescence imaging. Journal of the Science of Food and Agriculture (Apr 23. doi: 10.1002/jsfa.5702, Epub ahead of print).